SIMULTANEOUS SEPARATION, INTERPOLATION AND TUBE WAVE SUPPRESSION OF VERTICAL SEISMIC PROFILING USING MATCHING PURSUIT BASED SPARSE BEAM FORMING

JIANGTAO HU[1,2], JUNXING CAO[1,2], HUAZHONG WANG[3], XINGJIAN WANG[1], XUDONG JIANG[1,2]

[1] *State Key Laboratory of Oil and Gas Reservoir Geology and Exploitation, Chengdu University of Technology, 1 Dongsanlu, Erxianqiao, Chengdu 610059, Sichuan, P.R. China. jiangtao_hu@126.com*
[2] *College of Geophysics, Chengdu University of Technology, 1 Dongsanlu, Erxianqiao, Chengdu 610059, Sichuan, P.R. China*
[3] *WPI, School of Ocean and Earth Science, Tongji University, 1239 Siping Rd, Shanghai 200092, P.R. China.*

(Received June 17, 2017; revised version accepted December 10, 2017)

ABSTRACT

Hu, J.T., Cao, J.X., Wang, H.Z., Wang, X.J. and Jiang, X.D., 2018. Simultaneous separation, interpolation and tube wave suppression of vertical seismic profiling using matching pursuit based sparse beam forming. *Journal of Seismic Exploration*, 27: 117-135.

Since the vertical seismic profiling acquires seismic data with high resolution and superior S/N ratio, it is essential for reservoir monitoring in seismic exploration. The vertical seismic profiling data is usually separated into down-going and up-going wavefields in its processing procedure. The wavefield separation is mainly achieved by frequency-wavenumber method and plane wave decomposition method. However, when the vertical seismic profiling data is aliased, these methods perform poorly. Besides, to preserve the high frequency component during the wavefield separation, the data interpolation is required to avoid the aliasing effect of the signal. Furthermore, there is usually strongly aliased tube wave noise in the vertical seismic profiling data which poses challenge for the wavefield separation and subsequent processing steps. In this paper, we propose a solution using matching pursuit based sparse beam forming and it can simultaneously separate the wavefield, interpolate the data and suppress the tube wave noise. The matching pursuit based sparse beam forming is guided by the un-aliased information of the data. Thus, it can handle the aliasing effect of both signal and tube wave noise. Since the sparse beam forming method obtains beam forming result with superior resolution of the ray parameter, it can separate the wavefield and suppress the tube wave noise based on their differences in the ray parameter domain. Then the filtered

0963-0651/18/$5.00

data can be backward transformed to a denser grid for a better preservation of the high frequency component. Numerical examples on both synthetic and real data show that the proposed method works well in terms of wavefield separation, tube wave suppression and data interpolation.

KEY WORDS: wavefield separation, tube wave suppression, wavefield interpolation, vertical seismic profiling, sparse beam forming.

INTRODUCTION

Vertical seismic profiling (VSP) is an essential method in seismic exploration and it acquires seismic data in the borehole. Since the receiver is close to the reflector and the recorded seismic wave only travels though the weathering layer once, the VSP data is of high resolution and superior S/N ratio (Goetz et al., 2008). Besides, since the detailed characterization of the reservoir requires high resolution subsurface image, the high resolution seismic source (e.g., the frequency range of the source is 1.5-150 Hz) (Dean et al., 2013) is also adopted to further enhance the resolution of the VSP data. In the processing procedure of the VSP data, the up-going and down-going wavefields separation is the fundamental processing step (Moon et al., 1986; Freire and Ulrych, 1988; Blias, 2007). A high quality wavefield separation is important for subsequent processing steps, such as deconvolution (Blias, 2007), vector wavefield decomposition (Sun et al., 2009; Lou et al., 2013) and seismic imaging (Leung et al., 2013; Soni and Verschuur, 2013). However, the conventional wavefield separation method is inadequate for the high resolution VSP data. Furthermore, the strongly aliased tube wave noise poses challenge for the wavefield separation and subsequent processing steps (Hardage, 1981; Greenwood et al., 2012; Nadri et al., 2012).

There are several methods developed for VSP up-going and down-going wavefields separation, such as median filter method (Stewart, 1985), frequency-wavenumber (i.e., F-K) method (Treitel at al., 1967; Hu and McMechan, 1987; Liu et al., 2011; Hu et al., 2016), plane wave decomposition method (Moon et al., 1986), singular value decomposition filter method (Freire and Ulrych, 1988; Gao et al., 2014) and wave by wave separation method (Blias, 2007). The singular value decomposition filter method (Gao et al., 2014) and wave by wave separation method (Blias, 2007) separate the wavefield by iteratively estimating the velocity of each wave mode, flattening each wave mode and extracting each wave mode. These methods separate one wave mode per iteration. The F-K method and plane wave decomposition method (Hu and McMechan, 1987; Moon et al., 1986) are widely used. Since the up-going and down-going wavefields are separated after the F-K transform and plane wave decomposition, these methods can simultaneously separate all the wave modes. However, the F-K method and plane wave decomposition method cannot handle the aliasing effect and the high resolution VSP data is usually aliased at high frequency. Besides, since the tube wave travels along the borehole with slow velocity, it is strongly aliased which poses great challenge for the processing method.

There are two ways to handle the aliasing issue. The first one is to acquire the data with a small receiver interval. However, an ultra-small receiver interval (e.g., 3 m) is required to completely avoid the aliasing effect which greatly increases the cost of data acquisition (Greenwood et al., 2012). The alternative solution is to use processing method with strong ability of anti-aliasing. Besides, it is best to interpolate the data into a denser grid (i.e., smaller receiver interval) for a better preservation of the high frequency component (Xu et al., 2005). This is crucial for the detailed description of the reservoir (Goertz et al., 2008). Moreover, it is best to use the slope (i.e., angle or ray parameter) based method in wavefield separation because the tube wave noise and the signal has different slopes. Thus, the tube wave noise can be suppressed during the wavefield separation. Conventionally, the wavefield separation (Hu and McMechan, 1987), data interpolation (Liu and Sacchi, 2004) and tube wave suppression (Nadri et al., 2012) are regarded as separated processing steps in the processing procedure and each processing step requires different processing techniques.

In this paper, a solution to the above issues is proposed using matching pursuit based sparse beam forming (MPBF). The sparse beam forming has strong ability to address the aliasing issue and it can simultaneously separate the up-going and down-going wavefields, interpolate the VSP data and suppress the tube wave. Numerical examples on both synthetic and field data demonstrate the feasibility of the proposed method.

UP-GOING AND DOWN-GOING WAVEFIELD SEPARATION

The VSP acquires data by receiving the data in the borehole and firing the seismic source on the surface. Fig. 1 is a simplified illustration of the VSP data acquisition. There are many types of wave modes in VSP geometry, such as down-going direct wave, up-going reflection, up-going multiple, down-going multiple, etc. Each wave mode illuminates different areas of the subsurface. These wave modes can be generally categorized into down-going and up-going wavefields. Decomposing the VSP data into up-going and down-going wavefields is beneficial for separating each wave mode. It reduces the artefact in seismic imaging and velocity inversion (Leung et al., 2013; Soni and Verschuur, 2013). Besides, the three component (i.e., 3C) receiver is usually used in VSP acquisition. Decomposing the VSP data into up-going and down-going wavefields also helps the vector wave decomposition (i.e., compressional and shear wave decomposition) (Lou et al., 2013).

In the F-K domain, the up-going and down-going wavefields are defined as (Hu and McMechan, 1987; Liu et al., 2011; Hu et al., 2016),

$$d^{up}(\omega,k_z)=\begin{cases} d(\omega,k_z), \text{if } \omega k_z>0 \\ 0, \qquad \text{if } \omega k_z \le 0 \end{cases}, \tag{1}$$

$$d^{down}(\omega,k_z)=\begin{cases}0, & \text{if } \omega k_z \geq 0\\ d(\omega,k_z), & \text{if } \omega k_z < 0\end{cases}, \tag{2}$$

where, $d(\omega,k_z)$ is the Fourier transform of the VSP data; ω is the angular frequency; k_z is the wavenumber along depth z-axis. A similar expression can be obtained in the ray parameter p_z domain (i.e., plane wave decomposition method) using the following expression,

$$p_z = k_z / \omega. \tag{3}$$

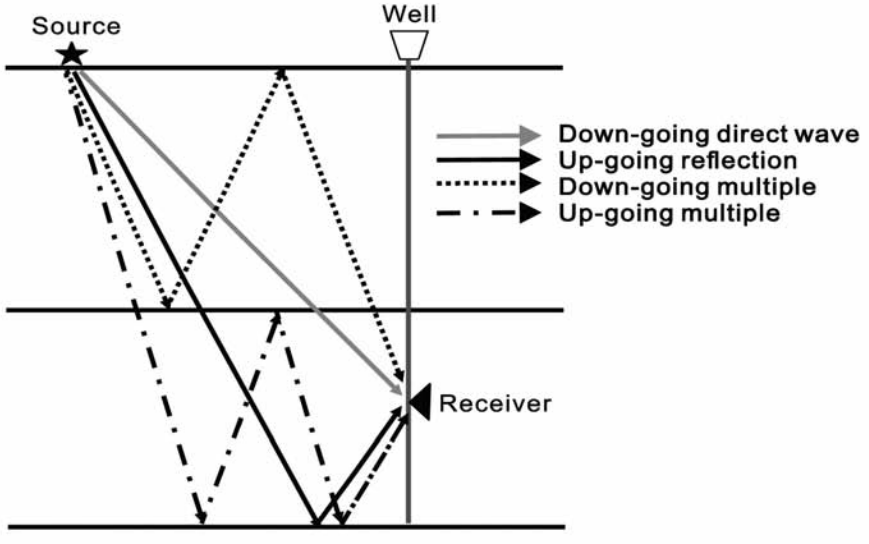

Fig. 1. The schematic illustration of VSP wave paths.

Since the F-K method and plane wave decomposition method are simple and efficient, they are widely used in VSP data processing. However, these methods are only appropriate for the un-aliased VSP data. Application of these methods to the aliased VSP data might distort the signal. The high resolution VSP data is usually aliased at high frequency. Since the velocity of shear wave is slower than the compressional wave, it might also be aliased. Besides, since the tube wave noise travels along the borehole with slow velocity, it is usually strongly aliased. Fig. 2 shows a real VSP data from a vibrator. The receiver interval is 20 m. There is strong tube wave in this data. In its F-K spectrum, the tube wave is strongly aliased and some weak signal is about to be aliased at 75 Hz. In the design of the acquisition strategy, the 20 m receiver interval limits the highest frequency of the seismic source to 90 Hz. This helps to avoid the aliasing effect but prevents us from using the high resolution seismic source (Dean et al., 2013). And the high frequency part might not be preserved during the imaging stage (Zhang

et al., 2003) due to the large receiver interval. Moreover, the aliasing effect makes the F-K method invalid. Take the down-going tube wave for example, its un-aliased part remains in the negative wavenumber area but its aliased part appears in the positive wavenumber area, as shown in Fig. 2(b). Therefore, if we apply eq. (2), the high frequency part of the down-going tube wave is lost. And some aliased up-going tube wave remains in the separated down-going tube wave. This phenomenon also applies to the signal. If the F-K method is applied to the signal, the high frequency part of the signal might also be damaged. This will be illustrated in the numerical examples. Therefore, method with strong ability of anti-aliasing is required to preserve the signal.

SPARSE BEAM FORMING FOR SEPARATION, INTERPOLATION AND TUBE WAVE SUPPRESSION

Since beam forming decomposes the local seismic data into their local plane wave components, it is widely used in seismic exploration, such as noise suppression (Ozbek, 2000) and migration (Gao et al., 2006). In a local spatial window, the seismic data can be regarded as the summation of local plane wave components,

$$d(\omega, z) = \sum_{p_z^i = p_{\min}}^{p_{\max}} m(\omega, p_z^i) e^{i\omega p_z^i (z - z_0)}, \tag{4}$$

where, m is the local plane wave component, z_0 is the location of beam center, $p_{\min}$ is the minimum ray parameter, $p_{\max}$ is the maximum ray parameter. Note that the ray parameter here is the local ray parameter instead of the global ray parameter. The conventional beam forming is usually achieved by local slant stack,

$$m(\omega, p_z) = \sum_{z^j = z_{\min}}^{z_{\max}} d(\omega, z^j) e^{-i\omega p_z (z^j - z_0)}, \tag{5}$$

where, $z_{\max} - z_{\min}$ is the beam width, $z_{\min}$ is the minimum receiver depth, $z_{\max}$ is the maximum receiver depth, z^j is the j-th receiver depth. But local slant stack suffers from leaked noise and low resolution (Sacchi and Ulrych, 1995; Trad et al., 2002). Besides, it is not amplitude preserving.

To improve the beam forming result, it is best to use sparse inversion in the beam forming process (Sacchi and Ulrych, 1995; Trad et al., 2002; Liu and Sacchi, 2004). Since the ray parameter may vary rapidly with receiver depth, it is hard to promote sparsity in the global plane wave decomposition. However, there are just few local plane wave components in a local temporal-spatial window and this makes the sparse inversion valid. The sparse inversion helps anti-aliasing (Liu and Sacchi, 2004). Eq. (4) can be written in matrix form,

$$\mathbf{d} = \mathbf{L}\,\mathbf{m} \quad , \tag{6}$$

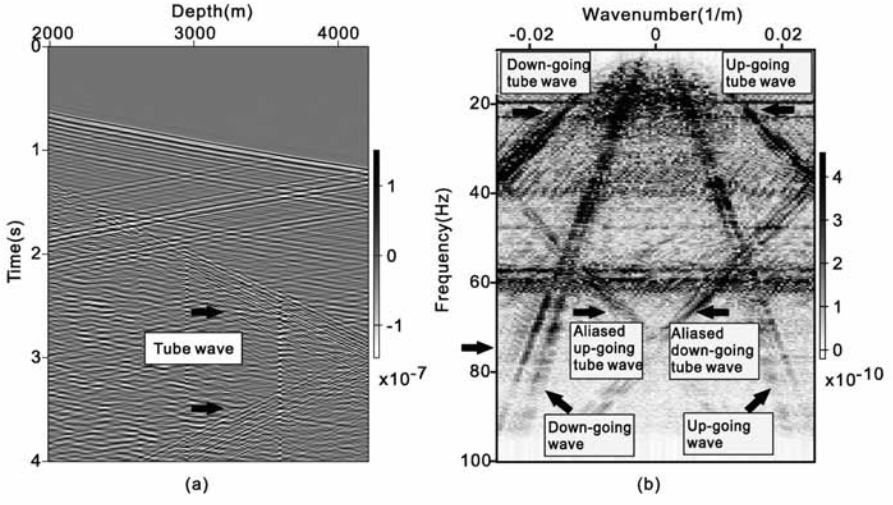

Fig. 2. The real VSP shot gather (a) and its F-K spectrum (b).

where **L** is the transformation matrix constructed by $e^{i\omega p_z(z-z_0)}$. The optimization problem of the sparse inversion is,

$$\begin{aligned} &\min : |\mathbf{m}|_0 \\ &s.t. : |\mathbf{Lm}-\mathbf{d}|_2^{\omega_{ref}} < \varepsilon, \end{aligned} \tag{7}$$

where, ε is the threshold which is used to judge the convergence of the inversion, ω_{ref} is a reference frequency range which is essential for anti-aliasing, *s.t.* means "subject to". This optimization problem uses the $l0$ norm as the model constraint which tries to get the sparsest solution (Elad, 2010). The optimization problem means to find the sparse solution which best matches the data in the reference frequency range. There are two reasons to choose the reference frequency range: (1) the seismic data may be contaminated by certain noise in certain frequency range and the selection of the reference frequency range may alleviate the influence of the noise; (2) the data may be aliased at high frequency. If the reference frequency range is dominated by the signal and free from aliasing effect, the signal dominates the beam forming process and the aliasing issue is avoided. In the VSP data processing, the reference frequency range should be free from the aliasing issue. Fig. 3 is a simplified synthetic VSP panel which contains up-going wavefield, down-going wavefield and strongly aliased tube wave (i.e., its slope is bigger). Its F-K spectrum in Fig. 3(b) shows that the wavefield is aliased at high frequency but it is not aliased at low frequency. To avoid the aliasing issue in the beam forming process, 15-40 Hz can be selected as the reference frequency range in this case. Other frequency range can also be selected as the reference frequency range once it does not contain the aliasing effect.

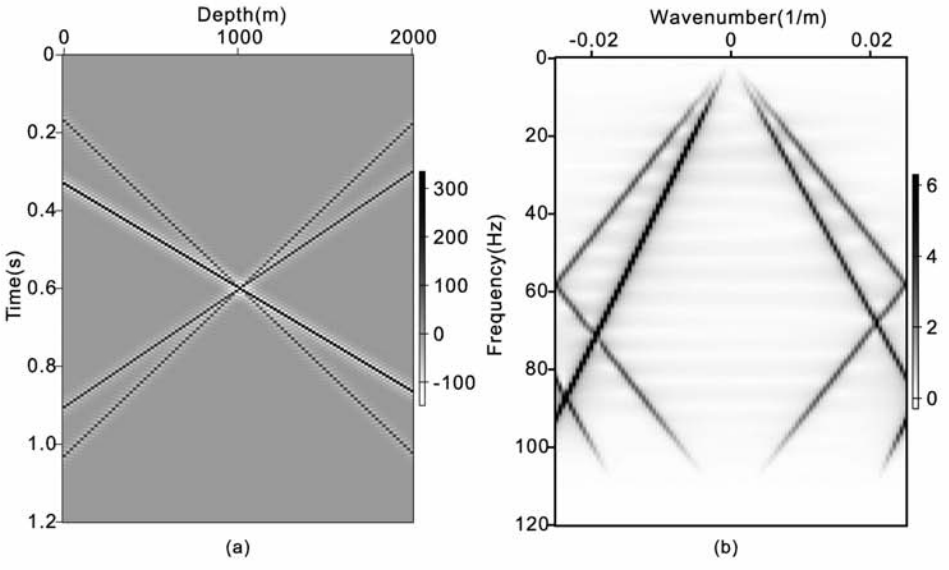

Fig. 3. The synthetic VSP shot gather (a) and its F-K spectrum (b).

We use matching pursuit method (Xu et al., 2005; Elad, 2010; Hu et al., 2016) to solve eq. (7) and it is briefly summarized as follows,

1. Initialize the solution of matching pursuit based beam forming (MPBF) to zero,

$$\mathbf{m}_0^{MPBF} = 0, \tag{8}$$

and set the residual data,

$$\mathbf{d}_0^{res} = \mathbf{d}. \tag{9}$$

2. The k-th iteration process begins.

2.1. Perform forward beam forming using the adjoint operator and residual data in the whole frequency range,

$$\mathbf{m}_k^{cad} = \mathbf{L}^H \mathbf{d}_k^{res}. \tag{10}$$

This is served as the candidate solution $\mathbf{m}_k^{cad}$ of k^{th} iteration (i.e., the dictionary of solution).

2.2. Compute the stack energy curve $A(p_z)$ in the reference frequency range by,

$$A(p_z) = \sum_{\omega_k=\omega_{\min}}^{\omega_{\max}} (m(\omega_k, p_z))^2, \tag{11}$$

where, $\omega_{\min}$ and $\omega_{\max}$ are the minimum and maximum frequencies of the defined reference frequency range, respectively.

2.3. Find the ray parameter $p_z^{\max}$ with maximum stack energy and update the beam forming result in the whole frequency range,

$$m_{k+1}^{MPBF}(\omega, p_z^{\max}) = m_k^{MPBF}(\omega, p_z^{\max}) + m^{cad}(\omega, p_z^{\max}) \quad . \tag{12}$$

2.4. Update the residual data by backward transforming the ray parameter with maximum energy and subtracting it from the residual data,

$$\mathbf{d}_{k+1}^{res} = \mathbf{d}_k^{res} - \mathbf{l}_{p_z^{\max}} m^{cad}(\omega, p_z^{\max}), \tag{13}$$

where,

$$\mathbf{l}_{p_z^{\max}} = \left[e^{i\omega p_z^{\max}(z^{\min}-z_0)} \quad . \quad e^{i\omega p_z^{\max}(z^j-z_0)} \quad . \quad e^{i\omega p_z^{\max}(z^{\max}-z_0)} \right]^T .$$

2.5. Judge whether the data residual $\sum_{\omega_k=\omega_{\min}}^{\omega_{\max}} \sum_{z^j=z_{\min}}^{z_{\max}} (d_{k+1}^{res}(\omega_k, z^j))^2$ drops below the threshold. If yes, the inversion process ends; If no, repeat step (2.1) to step (2.5).

The above beam forming method works in a moving window fashion and each window is moving with a half window overlap. It can provide beam forming result with superior resolution and the leaked noise is also suppressed. Besides, the aliasing issue is properly addressed and the result is amplitude preserving. This is good for the high resolution VSP data processing.

Wavefield separation

For the VSP data without tube wave noise, the down-going and up-going wavefields can be separated in the ray parameter domain by,

$$m^{up}(\omega, p_z) = m(\omega, p_z), \text{if } \omega p_z \geq 0, \tag{14}$$

$$m^{down}(\omega, p_z) = m(\omega, p_z), \text{if } \omega p_z < 0, \tag{15}$$

Then the backward beam forming using eq. (4) and the backward Fourier transform are required to transform the separated wavefields into the space-time domain.

Tube wave suppression

Since the tube wave travels with a slower velocity than the signal, its absolute value of ray parameter is usually bigger than the signal. Then the up-going and down-going wavefields with tube wave noise suppression can be denoted as,

$$m^{up}(\omega, p_z) = m(\omega, p_z), \text{if } \omega p_z^{fmax} > \omega p_z \geq 0, \tag{16}$$

$$m^{down}(\omega, p_z) = m(\omega, p_z), \text{if } \omega p_z^{fmin} < \omega p_z < 0, \tag{17}$$

where, p_z^{fmax} and p_z^{fmin} are the rejection ranges of the tube wave noise for the up-going and down-going wavefields, respectively.

Interpolation

The seismic data interpolation is one of the essential processing steps in seismic data processing and its key issues are anti-leakage and anti-aliasing (Liu and Sacchi, 2004; Xu et al., 2005). Since the sparse beam forming used in this paper has strong ability to suppress the leaked noise and handle the aliasing issue, the beam forming result can be backward transformed to any spatial location for the data interpolation purpose,

$$d(\omega, z^{sel}) = \sum_{p_z^i = p_{\min}}^{p_{\max}} m^f(\omega, p_z^i) e^{-i\omega p_z^i (z^{sel} - z_0)} \tag{18}$$

where, z^{sel} is the location of backward beam forming, m^f is the filtered result which can be either the up-going wavefield in eq. (16) or the down-going wavefield in eq. (17). Note that the location of backward beam forming should be within the beam width since the assumption of local plane wave is valid within the beam width.

NUMERICAL EXAMPLES

Synthetic data example

The synthetic data shown in Fig. 3 is tested in the first example. Fig. 4 shows the separated result using the F-K method. Since the space is limited, only the F-K spectrum of the up-going wavefield is shown. The result shows that the F-K method cannot separate the wavefield cleanly. There is a residual up-going wavefield in the separated down-going wavefield (horizontal arrow in Fig. 4(a)) and there is also a residual down-going wavefield in the separated up-going wavefield (horizontal arrow in Fig. 4(b)). The F-K method also has some boundary effect, as pointed out by the vertical arrow in Fig. 4(b). The F-K spectrum in Fig. 4(c) also shows that the high frequency component of the up-going wavefield is lost. This is because the high frequency component is aliased into the negative wavenumber area and eq. (1) cannot take that into account. Besides, the F-K method only separates the wavefield but it does not suppress the tube wave noise.

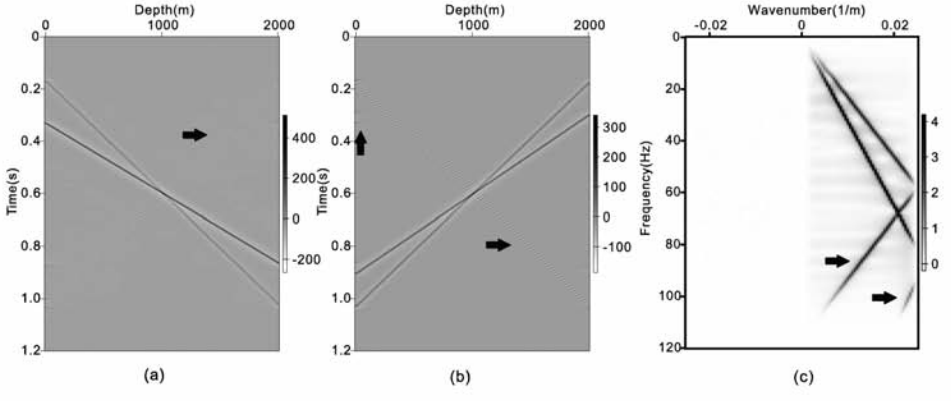

Fig. 4. The separated down-going wavefield (a), up-going wavefield (b) and F-K spectrum of up-going wavefield (c) using the F-K method.

Then the synthetic data is processed using the beam forming method. After analyzing the F-K spectrum in Fig. 3(b), 15-40 Hz is used as the reference frequency range for the sparse beam forming. The beam width is 2000 m and its beam center locates at 1000 m. Fig. 5 shows the beam forming results from local slant stack and sparse beam forming. The result of local slant stack suffers from low resolution and leaked noise which are not good for suppressing the tube wave noise. However, the result of the sparse beam forming shows superior resolution of the ray parameter and the leaked noise is also suppressed. After analyzing the beam forming result, -0.00035-0 (s/m) is selected as the ray parameter range of the down-going wavefield and 0-0.00035 (s/m) is selected as the ray parameter range of the up-going wavefield. The ray parameter outside these ranges is treated as the tube wave noise.

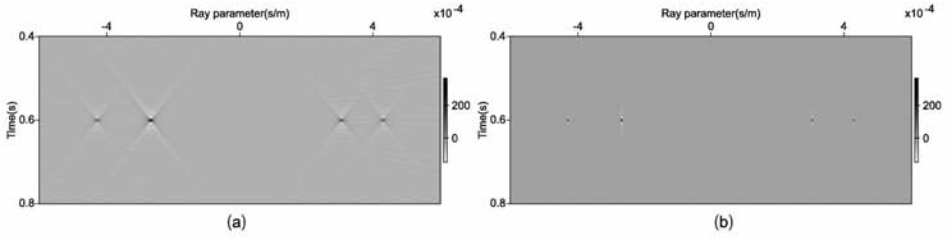

Fig. 5. The beam forming results from local slant stack (a) and sparse beam forming (b).

Fig. 6 is the separated result using local slant stack. It shows that the local slant stack performs poorly in wavefield separation. There is some residual tube wave noise and this is caused by the aliasing issue. Besides, the amplitude of the separated wavefield is different from the original data and the dominant frequency moves towards the low frequency. Fig. 7 is the separated result using sparse beam forming and it works well in wavefield separation. The tube wave noise is completely removed. This shows that the sparse beam forming has strong ability to handle the aliasing issue. Then the separated up-going and down-going wavefields are subtracted from the original data to get the removed tube wave noise, as shown in Fig. 8. There is no signal in the removed tube wave noise and this shows that the sparse beam forming is amplitude preserving.

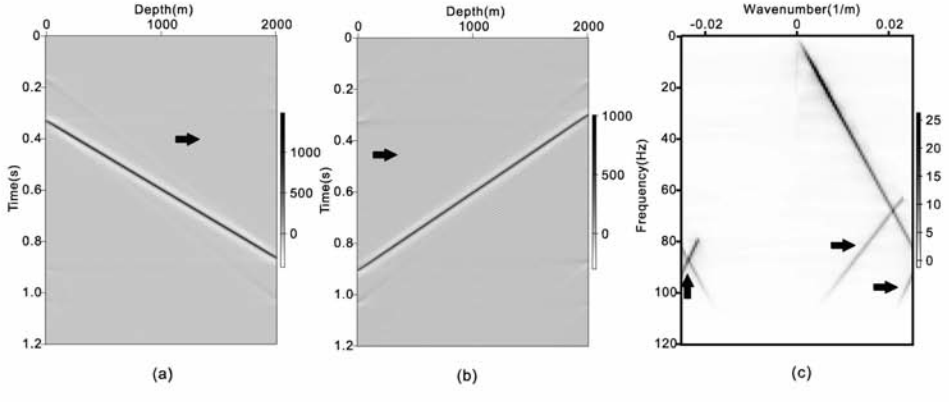

Fig. 6. The separated down-going wavefield (a), up-going wavefield (b) and F-K spectrum of up-going wavefield (c) using the local slant stack method.

Although the sparse beam forming performs well in wavefield separation and tube wave suppression, the separated down-going and up-going wavefields are still aliased at high frequency (as shown in Fig. 7(c)). In the subsequent processing steps [e.g., seismic imaging (Zhang et al., 2003)], this

aliased high frequency component might be lost. It is best to interpolate the data into a denser grid for preserving this high frequency component. Then we simultaneously separate the wavefield, interpolate the data into 10 m receiver interval and suppress the tube wave noise using the sparse beam forming. The result is shown in Fig. 9. It still performs well in wavefield separation and the tube wave is suppressed. Besides, the wavefield looks more continuous due to the smaller receiver interval and the aliased energy is corrected to the right place in the F-K spectrum [Fig. 9(c)]. Besides, we can use seismic source with broader bandwidth (Dean et al., 2013) without spending too much money in the data acquisition.

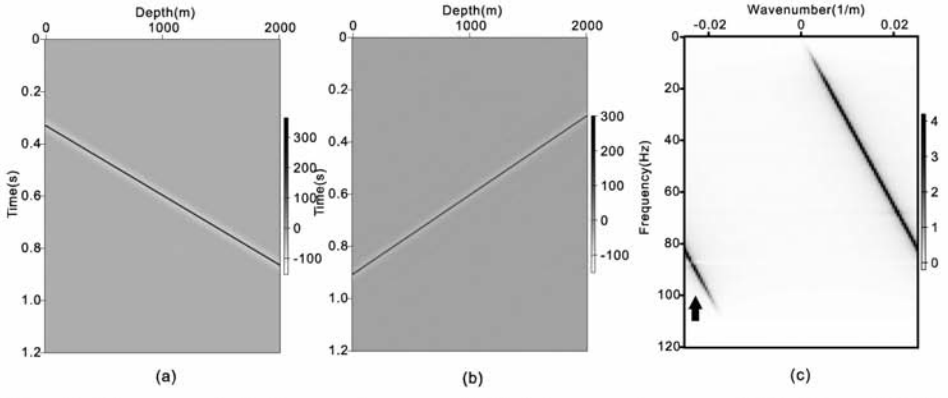

Fig. 7. The separated down-going wavefield (a), up-going wavefield (b) and F-K spectrum of up-going wavefield (c) using the sparse beam forming method.

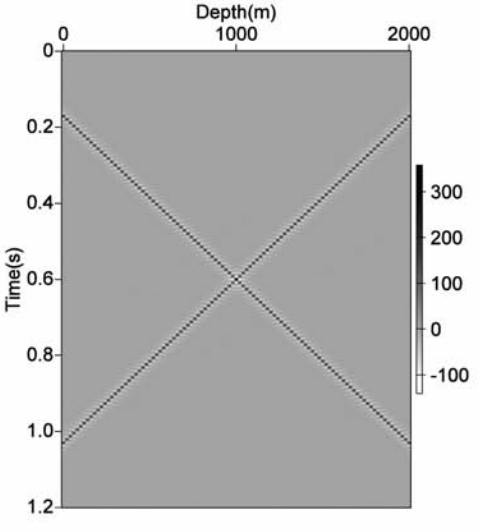

Fig. 8. The suppressed tube wave noise using the sparse beam forming method.

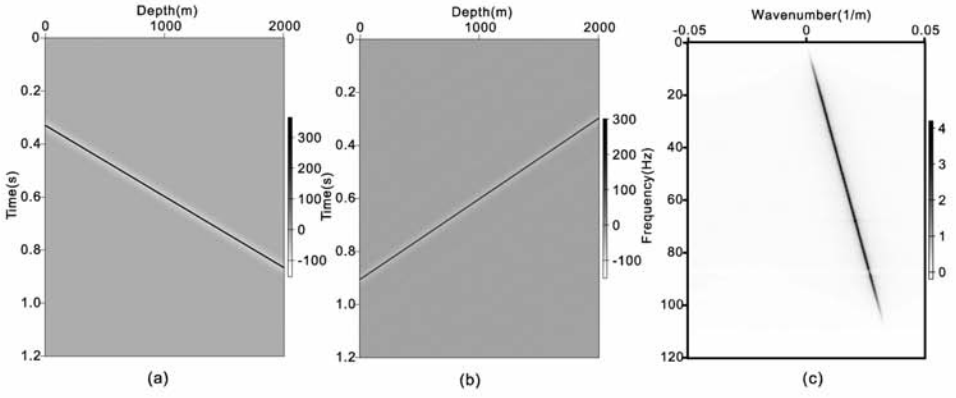

Fig. 9. The separated down-going wavefield (a), up-going wavefield (b) and F-K spectrum of up-going wavefield (c) using the sparse beam forming method. The receiver interval is interpolated to 10 m.

Real data example

Then the field data shown in Fig. 2 is further tested. Fig. 10 shows the separated result using the F-K method. It shows that the F-K method suffers from the boundary effect, as denoted by the arrow in Figs. 10(a) and 10(b). There is strong residual tube wave noise in the separated result, as denoted by the circle in Figs. 10(a) and 10(b). The F-K spectrum in Fig. 10(c) shows that there is low frequency up-going tube wave and high frequency down-going tube wave in the separated up-going wavefield. Since the tube wave noise is distorted by this processing step, it becomes hard to remove in the subsequent processing steps. We also find the weak event is not continuous, it will be shown later in the zoomed-in image.

Then we process the data using the beam forming method. 15-35 Hz is used as the reference frequency range for the sparse beam forming and the beam width is 400m. To show the advantage of the sparse beam forming, the beam forming results are compared first. Then the beam forming is performed with its beam center locating at 3200 m. Fig. 11 is the comparison of beam forming results. The result of local slant stack suffers from low resolution and strongly leaked noise due to the narrow beam width (Sacchi and Ulrych, 1995). In Fig. 11(a), the signal and the tube wave are not completely separated in the ray parameter domain. However, the result of the sparse beam forming is of superior resolution. In Fig. 11(b), the signal and tube wave have different ray parameter ranges. After analyzing the beam forming result, -0.0005-0 (s/m) and 0-0.0005 (s/m) are selected as the ray parameter ranges of down-going and up-going wavefields, respectively. To process the whole shot gather, the beam center moves from 2000 m to 4200 m with an increment of half beam width. Each beam center is processed in the same way to get the final result.

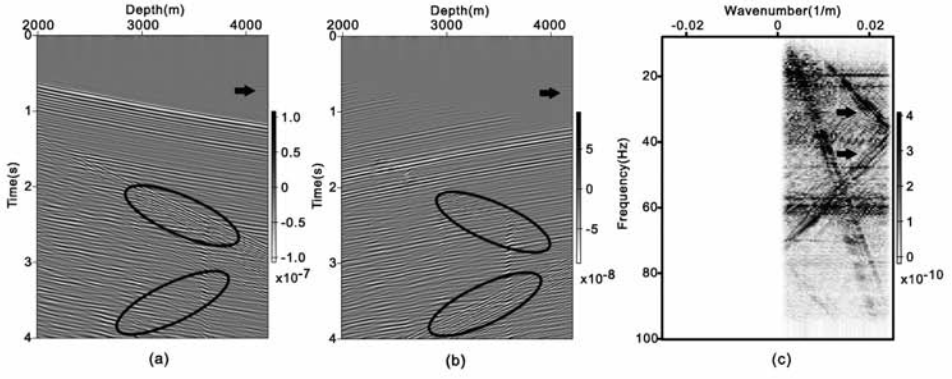

Fig. 10. The separated down-going wavefield (a), up-going wavefield (b) and F-K spectrum of up-going wavefield (c) using the F-K method.

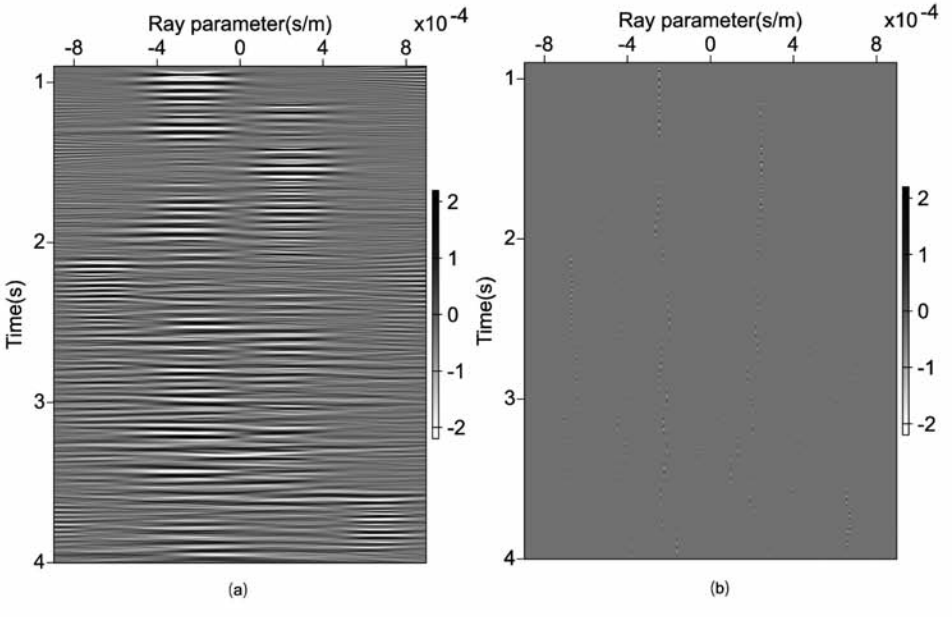

Fig. 11. The beam forming results from local slant stack (a) and sparse beam forming (b). The beam center is located at 3200 m and the beam width is 400 m.

Fig. 12 is the separated result using local slant stack method. It shows that the local slant stack method does not cleanly separate the wavefield and suppress the tube wave. For example, there are high frequency down-going wavefield and aliased down-going tube wave noise in the separated up-going wavefield, as shown in Fig. 12(c). This is caused by the aliasing issue. Fig. 13 is the separated result using sparse beam forming. It works well in terms

of separating the wavefield and suppressing the tube wave noise. Then the separated up-going and down-going wavefields are subtracted from the original data to get the suppressed tube wave, as shown in Fig. 14. There is almost no signal in the suppressed tube wave. This shows that the proposed method works well in terms of amplitude preservation. The weak event in the separated result of sparse beam forming is also not continuous and this will be shown in the zoomed-in image later. Then we simultaneously separate the wavefield, interpolate the wavefield into 10 m receiver interval and suppress the tube wave. Fig. 15 is the result. It still performs well in wavefield separation and tube wave suppression. The F-K spectrum shows that it allows us to use seismic source with much broader bandwidth since the receiver interval is smaller. This is beneficial for the high resolution data processing.

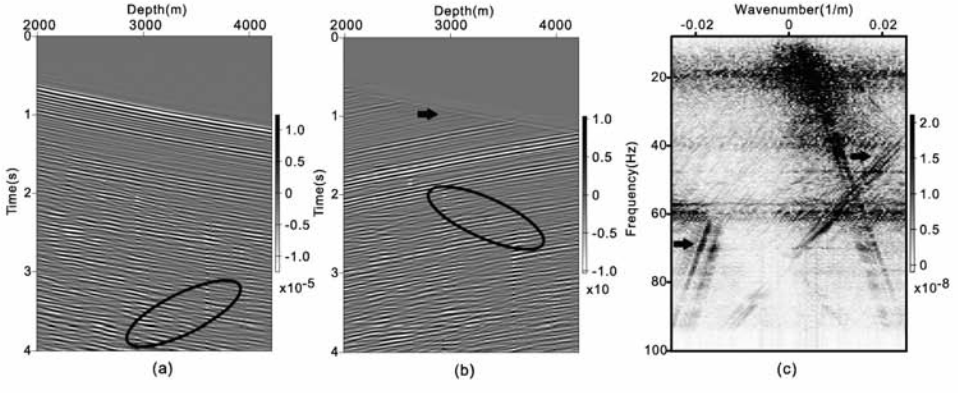

Fig. 12. The separated down-going wavefield (a), up-going wavefield (b) and F-K spectrum of up-going wavefield (c) using the local slant stack method.

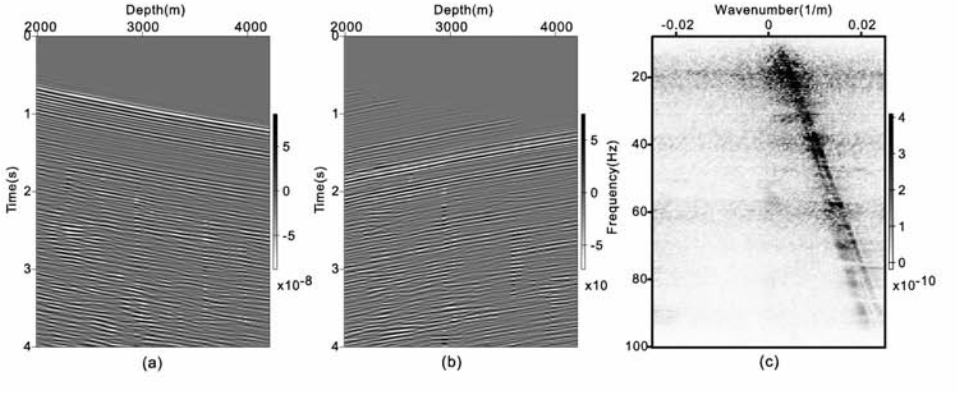

Fig. 13. The separated down-going wavefield (a), up-going wavefield (b) and F-K spectrum of up-going wavefield (c) using the sparse beam forming method.

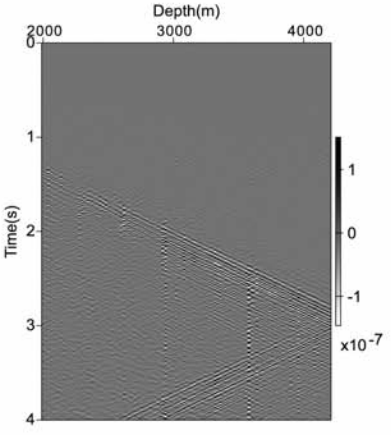

Fig. 14. The suppressed tube wave noise using the sparse beam forming method.

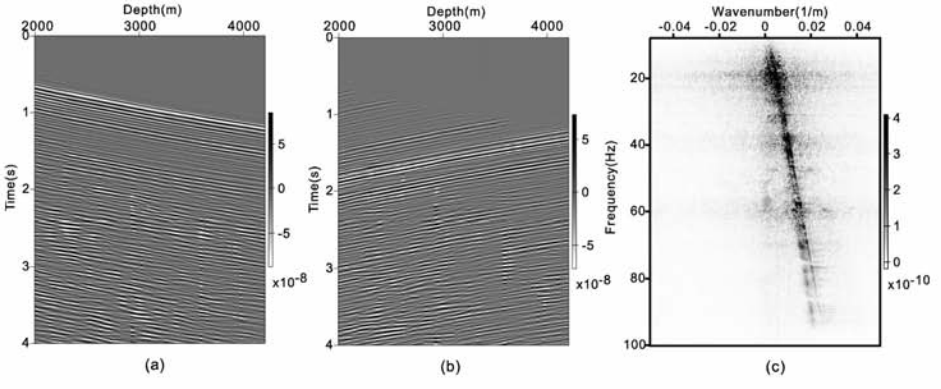

Fig. 15. The separated down-going wavefield (a), up-going wavefield (b) and F-K spectrum of up-going wavefield (c) using the sparse beam forming method. The receiver interval is interpolated to 10 m.

Fig. 16 shows the zoomed-in views of the separated up-going wavefields from different methods. The F-K method suffers from boundary effect (denoted by the vertical arrow in Fig. 16(a)) and the wavefield in the circle is affected by the tube wave noise. Besides, the weak event is not continuous due to the large receiver interval. In the result of local slant stack [Fig. 16(b)], there is some residual down-going wavefield and the weak event is not continuous. The result of sparse beam forming in Fig. 16(c) shows good wavefield separation and tube wave suppression but its weak event is still not continuous. The result of sparse beam forming with receiver interval interpolated to 10 m in Fig. 16(d) still shows good wavefield separation and tube wave suppression. Besides, the event is much more continuous. This helps to preserve the detailed information in the subsequent processing steps.

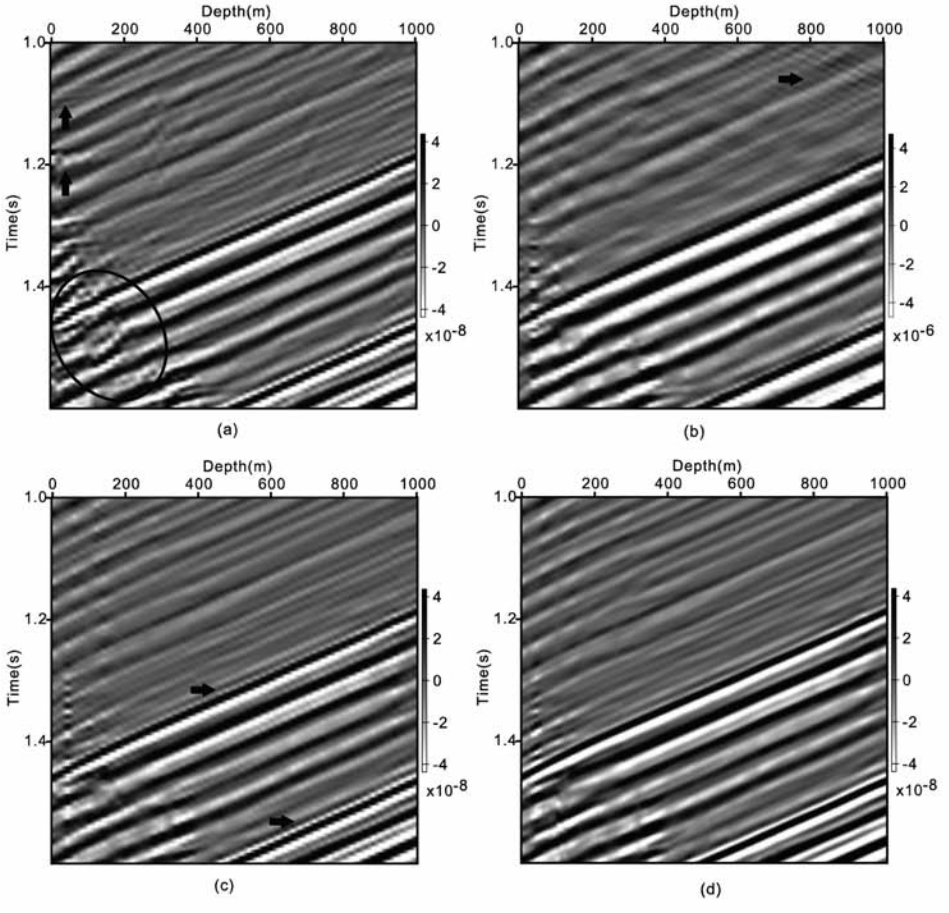

Fig. 16. The zoomed-in view of the separated up-going wavefield using F-K method (a), local slant stack method (b), sparse beam forming (receiver interval is 20 m) (c) and sparse beam forming (receiver interval is interpolated to 10 m) (d).

CONCLUSIONS

In this paper, a sparse beam forming based solution is proposed in VSP data processing which can simultaneously separate the wavefield into up-going and down-going wavefields, interpolate the data into a denser grid and suppress the strongly aliased tube wave noise. Since it uses the un-aliased information of the data to guide the beam forming process, it handles the aliasing effect of both signal and tube wave noise. It performs well in terms of wavefield separation and tube wave suppression due to its superior resolution of the ray parameter. It also interpolates the data into a denser grid which is essential for the broadband data processing in VSP. This can be treated as an alternative solution to the high density data acquisition which is quite expensive. Numerical examples show that the proposed idea works for both synthetic and real data.

The proposed method can be further extended into VSP vector wavefield decomposition to enable a better 3C processing of the VSP data.

ACKNOWLEDGEMENTS

This study is supported by the National Natural Science Foundation of China (NSFC, Grant No. U1562219, 41430323, 41604100, 41674112) and the National Key Research and Development Program (Grant No. 2016YFC0601100).

REFERENCES

Blias, E., 2007. VSP wavefield separation: wave-by-wave optimization approach. Geophysics, 72(4): T47-T55.

Dean, T., Tulett, J., Puckett, M., Lane, D., 2013. Improving land VSP resolution through the use of a broadband vibroseis source. Expanded Abstr., 83rd Ann. Internat. SEG Mtg., Houston: 5067-5071.

Elad, M., 2010. Sparse and Redundant Representations: From Theory to Applications in Signal and Image Processing. Springer Verlag, New York.

Freire, S.L. and Ulrych, T.J., 1988. Application of singular value decomposition to vertical seismic profiling. Geophysics, 53(6): 778-785.

Gao, F., Zhang, P., Wang, B., Dirks, V., 2006. Fast beam migration-a step toward interactive imaging. Expanded Abstr., 76th Ann. Internat. SEG Mtg., New Orleans: 2470-2473.

Gao, L., Chen, W.C., Wang, B.L. and Gao, J.H., 2014. VSP wave field separation: An optimization method based on block relaxation and singular value thresholding. J. Appl. Geophys. 104: 156-162.

Goetz, A., Chavarria, J.A., Paulsson, B., Karrenbach, M., Muller, K., Soroka, W., Marmash, S. and Al-Baloushi, M., 2008. Preservation of high frequencies in wide-aperture 3D VSP data from the Middle East. Expanded Abstr., 78th Ann. Internat. SEG Mtg., Las Vegas: 3345-3349.

Greenwood, A., Dupuis, C.J., Urosevic, M. and Kepic, A., 2012. Hydrophone VSP surveys in hard rock. Geophysics, 77(5): WC223-WC234.

Hardage, B.A., 1981. An examination of tube wave noise in vertical seismic profiling data. Geophysics, 46: 892-903.

Hu, J.T., Wang, H.Z. and Wang, X.W., 2016. Angle gathers from reverse time migration using analytic wavefield propagation and decomposition in the time domain. Geophysics 81(1): S1-S9.

Hu, L. and McMechan, G.A., 1987. Wave-field transformations of vertical seismic profiles. Geophysics, 52: 307-321.

Leung, V., Wong, M. and Zhang, R., 2013. Up- and Down-going wave multiples RTM imaging for VSP. Expanded Abstr., 83rd Ann. Internat. SEG Mtg., Houston: 5052-5056.

Liu, B. and Sacchi, M.D., 2004. Minimum weighted norm interpolation of seismic records. Geophysics, 69: 1560-1568.

Liu, F.Q., Zhang, G., Morton, S.A. and Leveille, J.P., 2011. An effective imaging condition for reverse-time migration using wavefield decomposition. Geophysics, 76(1): S29-S39.

Lou, M., Campbell, M., Cheng, D.J. and Doherty, F., 2013. An improved parametric inversion methodology to separate P and Sv wavefields from VSP data. Expanded Abstr., 83rd Ann. Internat. SEG Mtg., Houston: 5087-5091.

Moon, W., Carswell, A., Tang, R. and Dilliston, C., 1986. Radon transform wave field separation for vertical seismic profiling data. Geophysics, 51: 942-947.

Nadri, D., Urosevic, M., Wikes, P. and Asgharzadeh, M., 2012. Tube wave removal from vertical seismic profiling (VSP) surveys. Expanded Abstr., 22nd Internat. ASEG Conf., Melbourne: 1-4.

Ozbek, A., 2000. Adaptive beamforming with generalized linear constraints. Expanded Abstr., 80th Ann. Internat. SEG Mtg., Denver: 2081-2084.

Sacchi, M.D. and Ulrych, T.J., 1995. High-resolution velocity gathers and offset space reconstruction. Geophysics, 60: 1169-1177.

Soni, A.K. and Verschuur, D.J., 2013. Imaging blended VSP data using full wavefield migration. Expanded Abstr., 83rd Ann. Internat. SEG Mtg., Houston: 5046-5051.

Stewart, R.R., 1985. Median filtering: review and a new f/k analogue design. J. Can. Soc. Explor. Geophys., 1: 54-63.

Sun, W.B., Sun, S.Z. and Bai, H.J., 2009. 3C-3D VSP vector wavefield separation with constrained inversion. Expanded Abstr., 79th Ann. Internat. SEG Mtg., Houston: 4080-4084.

Trad, D., Ulrych, T. and Sacchi, M., 2002. Accurate interpolation with high resolution time-variant Radon transforms. Geophysics, 67: 644-656.

Treitel, S., Shanks, J.L. and Frasier, C.W., 1967. Some aspects of fan filtering. Geophysics, 32: 789-800.

Xu, S., Zhang, Y., Pham, D. and Lambaré, G., 2005. Antileakage Fourier transform for seismic data regularization. Geophysics, 70(6): V87-V95.

Zhang, Y., Sun, J.C. and Gray, S.H., 2003. Aliasing in wavefield exploration prestack migration. Geophysics, 68: 629-633.